Solution ^{1}H Nuclear Magnetic Resonance Determination of the Distal Pocket Structure of Cyanomet Complexes of Genetically Engineered Sperm Whale Myoglobin His^{64}(E7)→Val, Thr^{67}(E10)→Arg. The Role of Distal Hydrogen Bonding by Arg^{67}(E10) in Modulating Ligand Tilt

Jun Qin,* Gerd N. La Mar,* Francesca Cutruzzolá,‡ Carlo Travaglini Allocatelli,‡ Andrea Brancaccio,‡ and Maurizio Brunori‡

*Department of Chemistry, University of California, Davis, California 95616, USA, and ‡Department of Biochemical Sciences "A. Rossi Fanelli" and Consiglio Nazionale delle Ricerche Centre for Molecular Biology, University of Rome "La Sapienza," 00185 Rome, Italy

ABSTRACT Sequence-specific 2D methodology has been used to assign the ^{1}H NMR signals for all active site residues in the paramagnetic cyano-met complexes of sperm whale synthetic double mutant His^{64}[E7]→Val/Thr^{67}[E10]→Arg (VR-metMbCN) and triple mutant His^{64}[E7]→Val/Thr^{67}[E10]→Arg/Arg^{45}[CD3]→Asn (VRN-metMbCN). The resulting dipolar shifts for noncoordinated proximal side residues were used to quantitatively determine the orientation of the paramagnetic susceptibility tensor in the molecular framework for the two mutants, which were found indistinguishable but distinct from those of both wild-type and the His^{64}[E7]→Val single point mutant (V-metMbCN). The observed dipolar shifts for the E helix backbone protons and Phe^{43}[CD1], together with steady-state nuclear Overhauser effect between the E helix and the heme, were analyzed to show that both the E helix and Phe^{43}[CD1] move slightly closer to the iron to minimize the vacancy resulting from the His^{64}[E7]→Val substitution, as found in V-metMbCN (Rajarathnam, K., J. Qin, G. N. La Mar, M. L. Chiu, and S. G. Sligar. 1993. *Biochemistry.* 32:5670–5680). The dipolar shifts of the mutated Val^{64}[E7] and Arg^{67}[E10] allow the determination of their orientations relative to the heme, and the latter residue is shown to insert into the pocket and provide a hydrogen bond to the coordinated ligand, as found in the naturally occurring Val^{E7}/Arg^{E10} genetic variant, *Aplysia limacina* Mb. The oxy-complex of both *A. limacina* Mb and VR-Mb, VRN-Mb have been proposed to be stabilized by this hydrogen bonding interaction (Travaglini Allocatelli, C. et al. 1993. *Biochemistry.* 32:6041–6049). The magnitude of the tilt of the major magnetic axes from the heme normal in VR-metMbCN and VRN-metMbCN, which is related to the tilt of the ligand, is the same as in wild-type or V-metMbCN, but the direction of tilt is altered from that in V-metMbCN. It is concluded that the change in the direction of the ligand tilt in both the double and triple mutants, as compared to WT metMbCN and V-metMbCN single mutant, is due to the attractive hydrogen-bonding between Arg^{E10} and the bound cyanide.

INTRODUCTION

The differential ligation properties in natural genetic variants of myoglobin (Mb)[1] and hemoglobin (Hb) have been proposed to be controlled largely by the variable nature of two distal residues at the helical positions E7 and E11, both of which make contact with the bound ligand. The ubiquitous His (E7) of mammalian Mb provides a hydrogen bond to stabilize the coordinated oxygen molecule (Phillips et al., 1981), while His (E7) and/or Val (E11) provide steric interference to binding carbon monoxide (Phillips, 1980; Collman et al., 1976). The hydrogen bonding property manifests itself via a large O_2 binding constant that results from slow dissociation, while steric destabilization results in a strong tilt of the CO axis relative to the heme normal. The buccal muscle of the sea hare *Aplysia limacina* yields a Mb with Val instead of His at position E7, but with O_2 binding properties (Wittenberg et al., 1965), particularly a relatively slow O_2 off-rate, more closely resembling WT His (E7) containing sperm whale Mb than the His (E7) → Val point mutant (Springer et al., 1989). This has led to the proposal of an alternate mechanism of hydrogen bond stabilization of bound ligands in this invertebrate Mb, involving an Arg residue at helical position E10 (Bolognesi et al., 1989). X-ray crystallography of *A. limacina* metMbF, metMbN_3, and metMbCN has shown that Arg^{66}(E10) can readily insert into the pocket to hydrogen bond to the bound ligand (Bolognesi et al., 1990; Mattevi et al., 1991; Conti et al., 1993). In order to establish whether this alternate stabilization mechanism reflects solely on the nature of the side chains at position E7 and E10, the sperm whale double mutant His^{64}(E7) → Val, Thr^{67}(E10) → Arg has been prepared and, its oxygen binding properties have been determined (Cutruzzolá et al., 1991). While the single point mutant His^{64}(E7) →Val Mb leads to the expected strong decrease in O_2 binding constant via a significant increase in the O_2 off-rate (Springer et al., 1989),

Received for publication 7 May 1993 and in final form 10 August 1993.

Address reprint requests to Gerd N. La Mar.

[1] *Abbreviations used:* NMR, nuclear magnetic resonance; WT, wild type; Mb, myoglobin; SW, sperm whale; V-Mb, sperm whale single mutant Mb with His^{64}7)→Val; VR-Mb, sperm whale double mutant Mb with His^{64}-(E7)→Val, Thr^{67}(E10)→Arg; VRN-Mb, sperm whale triple mutant Mb with His^{64}(E7)→Val, Thr^{67}(E10)→Arg, Arg^{45}(CD3)→Asn; metMbCN, cyanomet myoglobin; NOE, nuclear Overhauser effect; MbCO, carbonmonoxy myoglobin; 2D, two dimensional; NOESY, two-dimensional nuclear Overhauser effect spectroscopy; COSY, two-dimensional bond correlation spectroscopy; MCOSY, magnitude COSY; TOCSY, two-dimensional total correlation spectroscopy; DSS, 2,2-dimethyl-2-silapentane-5-sulfonic acid; ppm, parts per million; WEFT, water-eliminated Fourier transform.

0006-3495/93/11/2178/13 $2.00

the additional Thr^{67}(E10)→Arg substitution leads to a substantial recovery of the O_2 binding affinity through a reduction of the O_2 off-rate to a value intermediates between that of WT and of His^{64}(E7)→Val Mb.

The cyanide ligand bound to the ferric form of metMb can serve as both a structural and functional model for several aspects of the control of ligand binding. The Fe^{+3}-CN unit is polar, and in sperm whale metMbCN serves as a hydrogen bond acceptor to His^{E7}, as does the Fe^{+2}-O_2 unit in MbO_2 (Lecomte and La Mar, 1987; Qin et al., 1992). Moreover, the Fe^{+3}-CN unit prefers to be linear and bound normal to the heme like the Fe^{+2}-CO unit, and hence the nature of the Fe^{+3}-CN tilt provides information on steric interactions in the distal pocket (Emerson and La Mar, 1990b; Rajarathnam et al., 1992; Qin et al., 1993). The kinetics of the cyanide off-rate upon rapid reduction of metMbCN also have been shown to be modulated by distal hydrogen bonding, and the retarded off-rate in reduced *A. limacina* metMbCN similarly has been interpreted in terms of distal hydrogen bonding by Arg^{E10} (Bellelli et al., 1990). The advantage of using the CN^- ligand as a probe in metMb, aside from obviating problems from autoxidation, is that it serves as a probe for both hydrogen bonding and steric interactions, and these interactions can be characterized in remarkable detail by solution ^{1}H NMR spectroscopy.

The hyperfine field due to the paramagnetic iron(III) leads to significant chemical shift dispersion for which the temperature-sensitive hyperfine shifts readily identify active site residues even in the presence of a large number of signals from proton distant from the active site (Emerson and La Mar, 1990a; Yu et al., 1990; Qin and La Mar, 1992). Most importantly, the paramagnetism imparts large shifts and strong relaxation to the labile protons of a distal residue that can be demonstrated to result from hydrogen bonding with bound ligand via the detection of an isotope effect on the heme contact shifts (Lecomte and La Mar, 1987; Qin et al., 1992). The hyperfine or dipolar shifts for the noncoordinated residues, together with crystal coordinates, yield the orientation of the magnetic susceptibility tensor whose major axis is determined by the Fe-CN tilt (Emerson and La Mar, 1990b; Rajarathnam et al., 1992, 1993). While the paramagnetism leads to some line broadening as well as hyperfine shifts, detailed studies of WT sperm whale metMbCN and three point mutants (Emerson and La Mar, 1990a; Yu et al., 1990; Rajarathnam et al., 1992, 1993) have shown that the line broadening does not interfere with the efficacy of two-dimensional (2D) NMR methods for defining solution structure. Hence, heme pocket residues were uniquely identified by their spin connectivity patterns and geometrically placed in the heme cavity via the detailed dipolar connectivities with the heme and with each other. Such assignments in *A. limacina* metMbCN, moreover, were shown to be attainable by standard sequence-specific methods by tracing the backbone of heme pocket residues (Qin and La Mar, 1992). Both the orientation of the magnetic susceptibility tensor and its anisotropy could be accurately determined for sperm whale metMbCN by fitting the observed dipolar shifts from noncoordinated residues using the WT MbCO crystal coordinates (Emerson and La Mar, 1990b). The major magnetic axis was found essentially colinear with the Fe-C bond in SW MbCO (Cheng and Schoenborn, 1991). Moreover, it was shown that the dipolar shifts and crystal coordinates of solely proximal side residues quantitatively described the tensor orientation in metMbCN (Rajarathnam et al., 1992). Subsequently, the dipolar shifts and crystal coordinates of the conserved proximal residues have been shown to accurately provide the orientation of the tensor in several distal point mutants. The changes in tensor orientation in these mutants could be related to changes in orientation of the Fe-CN unit that are consistent with expectation based on the crystal structure (Rajarathnam et al., 1992, 1993).

We report herein on the ^{1}H NMR spectrum of sperm whale double mutant His^{64}(E7)→Val, Thr^{E7}(E10)→Arg, metMbCN (VR-metMbCN), and the triple mutant His^{64}(E7)→Val, Thr^{67}(E10)→Arg, Arg^{45}(CD3)→Asn metMbCN (VRN-metMbCN). In the latter protein, Arg^{45} on the CD loop (CD3), which makes a salt bridge to the 6-propionate in WT MbCO, has been replaced to minimize potential coulombic repulsion with Arg^{67}(E10) (Travaglini Allocatelli et al., 1993). Preliminary ^{1}H NMR data on both mutants have identified a strongly relaxed labile proton in the distal cavity that hydrogen bonds to the bound ligand and induces an isotope effect on heme hyperfine shifts. Limited 2D studies identified the side chain as Arg^{67}(E10) and located the resonances for the distal pocket residue E5–E14. We extend here our sequence-specific assignments to all residues in the active site that exhibit hyperfine shifts, determine the orientation of the magnetic susceptibility tensor using the proximal side residues, and use this susceptibility tensor to both determine the orientation of the substituted Arg^{67}(E10) residue as well as assess other structural consequences of the substitutions on the distal pocket. The incremental influences of the Arg^{67}(E10) and Arg^{45}(CD3) substitutions are evaluated by detailed comparison with the ^{1}H NMR data recently reported for the single point mutant His^{64}(E7)→Val metMbCN (V-metMbCN) (Rajarathnam et al., 1993).

MATERIALS AND METHODS

Preparation of mutants

Mutagenesis was performed as already described in detail in Travaglini Allocatelli et al. (1993).

^{1}H NMR measurements

Cyano-met myoglobin complexes of mutants, metMbCN, were prepared by exchanging the oxidized protein on an Amicon ultrafiltration device with a solution of ^2H_2O or 10% ^2H_2O/90% ^1H_2O containing 0.1 M phosphate buffer, 0.02 M KCN, pH 7.0. The final concentrations for the sample are ~2 mM in ^2H_2O and ~4 mM in 10% ^2H_2O/90% ^1H_2O.

All ^{1}H NMR spectra of cyanide derivatives of mutants were collected on a GE Ω 500 MHz spectrometer. The steady-state nuclear Overhauser effect, NOE, spectra, SUPERWEFT spectra, and the nonselective spin-lattice

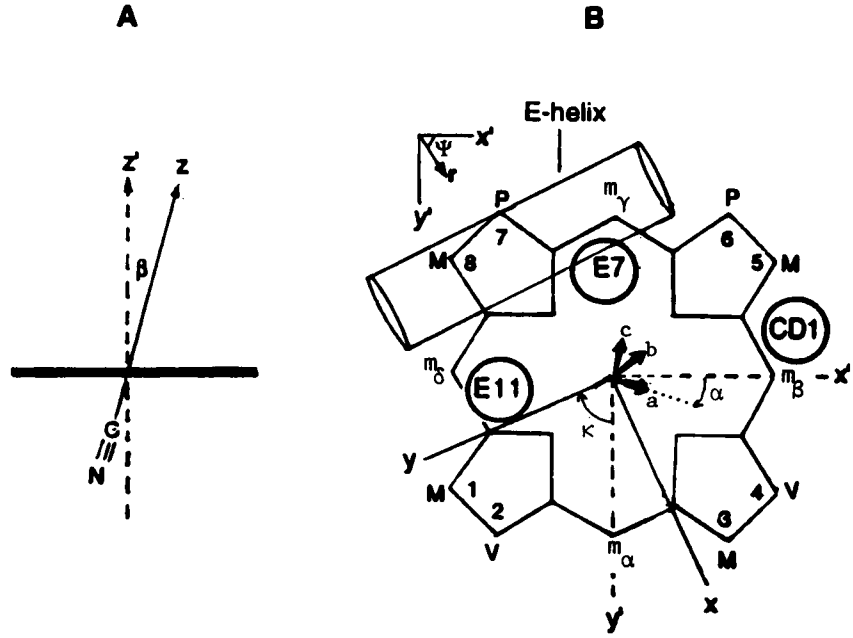

FIGURE 1 Orientation of the coordinate system, x, y, z, for the magnetic susceptibility tensor χ, relative to the symmetry (x-ray crystallographic) coordinate system x', y', z': (*A*) Tilt of the major magnetic axes, z, from the heme normal, z', given by the angle β; note that since the z axis is positive on the proximal side, the Fe-CN tilt is defined by the $-z$ axis. (*B*) Projection of the tilt of the z axis on the heme plane, defined by the angle α from the symmetry coordinate system x' axis, and location of the rhombic magnetic axes, x, y, whose projection on the heme plane is related to the symmetry axes, x', y', by the angle $\kappa \cong \alpha + \gamma$, where α, β, and γ are the Euler angles that transform the symmetry coordinates into the magnetic coordinates. The angle ψ, and modulus **r** define lateral movement of the E helix and Phe CD1. The arrows labeled *a*, *b*, and *c* correspond to the Fe-CN orientation in WT, V-metMbCN, and VR-metMbCN, respectively.

paramagnetic relaxation times for the resolved peaks were obtained as previously described (Emerson and La Mar, 1990a). The phase-sensitive HOHAHA or TOCSY (Braunschweiler and Ernst, 1983; Davis and Bax, 1985), NOESY (Jeener et al., 1976), and conventional *n*-type COSY (MCOSY) (Bax et al., 1984) employed the method described by States et al. (1982) to provide quadrature detection in the t1 dimension. The MLEV-17 mixing scheme (Bax and Davis, 1985) is used in the TOCSY experiments, and the MLEV-17 pulse is written in such a way so that the magnetization is aligned along the effective axis of rotation of 180° composite pulse to obtain optimal sensitivity (Rance, 1987). Solvent suppression, when required, was achieved by direct saturation in the relaxation delay period. 512 blocks were collected with two different spectral widths for all the 2D experiments, 23,255 Hz to include all proton resonances, and 15,000 Hz to improve resolution for the unresolved amino acid resonances for better resolution. 96–512 scans were accumulated for each block with free induction decays of 2048 complex points. The two repetition rates were used for all 2D experiments: 3 s^{-1} to emphasize the broad cross peaks (512 scans per block) and 0.7 s^{-1} to emphasize the weakly relaxed cross peaks (96 scans per block). The data were processed as previously described (Qin and La Mar, 1992); details are given in the figure captions.

Magnetic axes determination

The magnetic axes were determined as described in detail previously (Emerson and La Mar, 1990b; Rajarathnam et al., 1992, 1993). Experimental dipolar shifts for the structurally conserved proximal side of the heme were used as input to search for the Euler rotation angles, $R(\alpha, \beta, \gamma)$, that transform the molecular pseudo-symmetry coordinates, x', y', z', or r, θ', Ω', (see Fig. 2) (readily obtained from crystal coordinates) into magnetic axes, x, y, z, by minimizing the following error function:

$$F/n = \sum^{n} | \delta_{dip}(\text{obs}) - \delta_{dip}(\text{calc})F(\alpha, \beta, \gamma)|^2, \quad (1)$$

where

$$\delta_{dip}(\text{calc}) = -\frac{1}{3N}[\Delta\chi_{ax}(3\cos^2\theta' - 1)r^{-3} + \tfrac{3}{2}\Delta\chi_{rh}\sin\theta'\cos 2\Omega' r^{-3}], \quad (2)$$

and

$$\delta_{dip}(\text{obs}) = \delta_{obs} - \delta_{dia}. \quad (3)$$

$\Delta\chi_{ax}$ and $\Delta\chi_{rh}$ are axial and rhombic anisotropies, and δ_{obs} is the observed chemical shift referenced to DSS. δ_{dia} is the shift in the isostructural diamagnetic MbCO complex (Dalvit and Wright, 1987; Chiu, 1992), or calculated for protons whose δ_{dia} are not available by using the equation (Qin et al., 1993):

$$\delta_{dia} = \delta_{sec} + \delta_{rc}, \quad (4)$$

where δ_{sec} is the shift of an amino acid proton typical for α-helices, β-strand, coils, etc. (Wishart et al., 1991), and δ_{rc} is the heme-induced ring current shift of the proton based on the WT coordinates by using the eight loop model (Cross and Wright, 1985). Minimizing the error function F/n in Eq. 1 was performed over three parameters, α, β, γ, using available $\Delta\chi_{ax}$ and $\Delta\chi_{rh}$, or extended to all five parameters to yield both the Euler angles and anisotropies, as described in detail previously (Emerson and La Mar, 1990b; Rajarathnam et al., 1992).

Dipolar shift simulations

The position of a perturbed distal structural element was determined by minimizing a local error function for a selected set of protons (i.e., backbone for a helix or side chain protons for a residue) as influenced by controlled local movements. This local error function, designated F^*/n to distinguish it from that global error function in Eq. 1, is given by Rajarathnam et al. (1993):

$$F^*/n(i) = \sum^{n} | \delta_{dip}(\text{obs}) - \delta_{dip}(\text{calc})|^2. \quad (5)$$

Both δ_{dia} (Eq. 4) and δ_{dip}(calc) (Eqs. 1 and 2) are evaluated using the perturbed coordinates and the magnetic axes obtained from the conserved proximal side protons, as described above.

RESULTS

Assignments

The 500-MHz ^{1}H NMR spectra of VR-metMbCN in ^2H_2O and ^1H_2O at 25°C, pH 7.0, are illustrated in Fig. 2, *A* and *B*, respectively. The spectrum in ^2H_2O collected under rapid pulsing conditions to emphasize broad, rapidly relaxed protons is shown in Fig. 2 *C*. The target residues whose assignment are necessary to determine the magnetic axes are

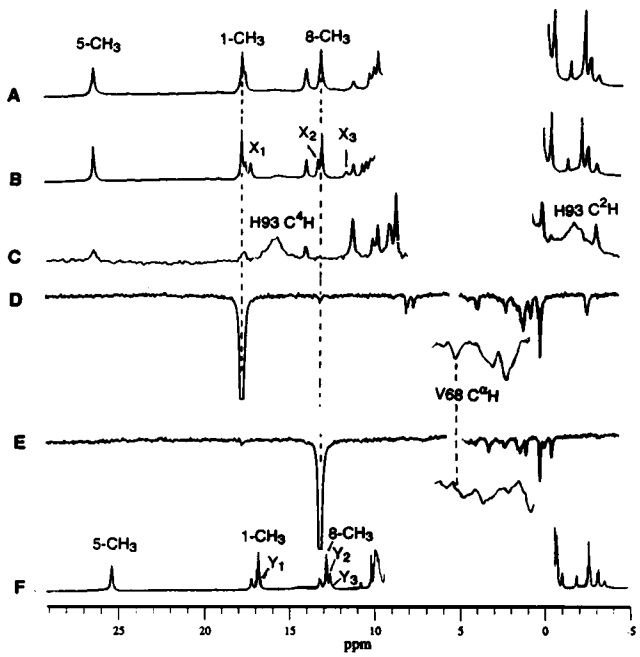

FIGURE 2 Hyperfine-shifted portions of the 500-MHz ^1H NMR reference spectra of VR-metMbCN at 25°C at pH 7.0 (*A*) in ^2H_2O; (*B*) in ^1H_2O; three resolved labile proton signals are labeled X_1, X_2, and X_3. (*C*) Rapid-repetition rate inversion-recovery spectrum in ^2H_2O collected at 15 s^{-1}; which emphasize broad, efficiently relaxed proton signals. (*D*) Steady-state NOE difference spectrum upon irradiating1-CH_3 in ^2H_2O. (*E*) Steady-state NOE difference spectrum upon irradiating 8-CH_3 in ^2H_2O; note much smaller NOE to Val E11 $C_\alpha H$ in *E* than *F* in the insets. (*F*) 500-MHz reference spectrum of VRN-metMbCN in ^2H_2O at 25°C and pH 7.0.

the proximal residues on the F helix, the FG corner, and one on the H helix[2] (Rajarathnam et al., 1992). The ^1H NMR spectra of VR-metMbCN (Fig. 1 *A*) and VRN-metMbCN (Fig. 1 *F*) are very similar, and previous limited assignments of E helix residues have shown that the two mutants exhibit essentially the same hyperfine shifts. Because of the very similar hyperfine shifts and essentially identical NOESY data, detailed 2D NMR data relevant to assignment and structure are presented only for VR-metMbCN. The strong similarity of the molecular structure of the two mutants is reflected in the very similar shifts listed in Tables 1 and 2.

The heme resonances are assigned in order to aid in assessing the structural perturbations due to the mutations. The E helix side chains in the distal pocket have been assigned previously (Travaglini Allocatelli et al., 1993); hence, only Phe[43](CD1) in the distal pocket of VR-metMbCN remains to be assigned.[3] Two three-spin and two four-spin systems involving only nonexchangeable strongly hyperfine shifted resonances exhibit COSY patterns characteristic of heme vinyl and propionate groups, respectively (not shown). The NOESY cross peaks to the heme methyls and meso-H signals, shown in Fig. 3, locate all heme resonances in a well documented manner (Emerson and La Mar, 1990a; Rajarathnam et al., 1992). The fingerprint region of the NOESY map locates a series of six sequential NH_i-NH_{i+1} connectivities, for which some NHs exhibit significant dipolar shift (Fig. 4 *B*). The COSY map in Fig. 4 *A* locates the $C_\alpha Hs$ for each residue, and tracing the remainder of the spin system (Fig. 5, *A* and *B*) over a range of temperature yields the fragment; Leu_i-Ala_{i+1}-Z_{i+2}-AMX_{i+3}-AMX_{i+4}-Ala_{i+5}. The sequence uniquely identifies the residues 89–94 corresponding to helical positions F4–F9. The relevant NOESY cross peaks are shown in Fig. 3 and reveal intra-residue and residue-heme dipolar connectivities as observed in WT (Emerson and La Mar, 1990a). The single labile proton peak at 17 ppm yields an NOE to the $NpepH_{i+3}$ (His[93](F8)), identifying it as the His[F8] ring N_1H. Steady-state NOEs from the broad peak at 15 ppm to the His[93](F8) $C_\beta Hs$, and from the broad peak at −2.5 ppm to the His[93](F8) N_1H (not shown), identify the His[93](F8) ring C_4H and C_2H signals, respectively, as reported for a variety of metMbCN complexes (Emerson and La Mar, 1990a; Rajarathnam et al., 1992; Qin and La Mar, 1992). Ile[99](FG5) gives rise to the furthest upfield and characteristically relaxed (T_1 ~70 ms) single proton peak that arises from $C_\gamma H$. The COSY (Fig. 5 *B*) and NOESY (Fig. 3) cross peaks within the residue, and the NOESY cross peak to the heme and to His[93](F8) are essentially the same as observed in WT. A rapidly relaxed (T_1 ~20 ms) single proton peak at 8.50 ppm exhibits a NOE to His[F8] $C_\alpha H$ which identifies it as His[97](FG3) C_4H; the NOESY cross peak from the 6-H_α to the aromatic region locates the His[FG3] C_2H (Fig. 3). TOCSY cross peaks among three resonances in the aromatic region (not shown), together with the NOESY cross peak to the heme 1-CH_3 and 2-H_α, (Fig. 3) locate the ring protons of Phe[138](H15). This completes assignment of the target proximal residues.

TABLE 1 ^1H NMR chemical shifts for heme resonances of sperm whale VR-metMbCN and VRN-metMbCN

	δ_{obs}*			δ_{obs}*	
Peak	VR	VRN	Peak	VR	VRN
1-CH_3	17.78	16.66	6-H'_α	6.37	9.55
3-CH_3	5.85	5.90	6-H_β	2.70	2.04
5-CH_3	26.01	25.24	6-H'_β	1.02	0.84
8-CH_3	12.63	12.81	7-H_α	2.67	3.40
2-H_α	17.15	17.12	7-H'_α	−0.65	−0.15
2-$H_{\beta c}$	−3.06	−3.10	7-H_β	−1.05	−1.06
2-$H_{\beta t}$	−3.14	−3.20	7-H'_β	0.48	0.29
4-H_α	5.14	5.12	α-meso-H	4.78	4.75
4-$H_{\beta c}$	−2.78	−2.67	β-meso-H	1.87	1.82
4-$H_{\beta t}$	−1.93	−1.89	γ-meso-H	4.77	4.73
6-H_α	13.45	9.61	δ-meso-H	0.75	0.94

* Shifts in ppm referenced to DSS, in ^1H_2O, 0.2 M in NaCl, pH 7.0, and 25°C.

[2] The nine-proton input set **I** (references to set E in Rajarathnam et al., 1992), includes; $C_\alpha H$ of Leu[89](F4); $C_\delta H$, $C_\epsilon H$ of His[97](FG3); $C_\alpha H$, $C_\beta H$, $C_{\gamma 1} H$, $C_{\gamma 2} H$, $C_\gamma H_3$, $C_\delta H_3$ of Ile[99](FG5). The 14-proton input data set **II** (referenced to as set D′ in Rajarathnam et al., 1992) has, in addition to the nine protons identified above, $C_\alpha H$, $C_\beta H_3$ of Ala[F5] and $C_\zeta H$, $C_\epsilon Hs$, $C_\delta Hs$ of Phe[138](H15) (referred to set D′ in Rajarathnam et al., 1992).

[3] The assignment for other distal residue not used in the determination of magnetic axes are for: Phe[33](B14), $C_\delta H$ 7.24, $C_\epsilon Hs$ 7.12, $C_\zeta H$ 8.20; Phe[43](CD1), $C_\beta H$ 3.65, $C_\beta H'$ 2.85, $C_\alpha H$ 4.67; Phe[46](CD4) $C_\delta Hs$ 7.39, $C_\epsilon Hs$ 7.30, $C_\zeta H$ 7.43 ppm.

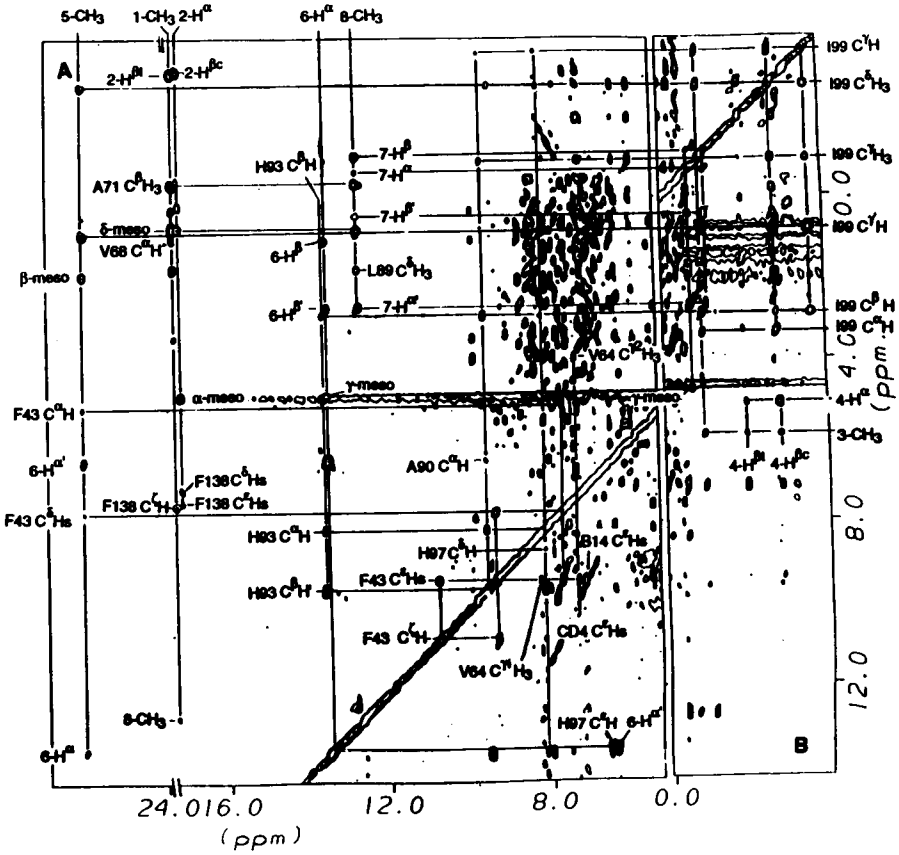

FIGURE 3 Resolved (*A*) lowfield and (*B*) upfield portions of the NOESY spectrum (mixing time 50 ms) of VR-metMbCN in ^2H_2O, pH 7.0, at 25°C illustrating the important cross peaks for the heme and hyperfine-shifted residue protons, as well as between protons of different residues and to the heme. The data were processed by applying a 30°-shifted sine-bell-squared window over 512 t1 × 512 t2 points prior to zero-filling to 2048 × 2048 data points and Fourier transformation.

The side chain for the E helix residues have been previously assigned sequence specifically, and the shifts for signals exhibiting dipolar shifts >1 ppm are listed in Table 2. The strongly relaxed (T_1 ~20 ms) low field single proton peak which COSY identifies as part of an AM_2X_2 spin system (Fig. 5 *A*) arises from a rapidly rotating phenyl ring; the characteristic NOESY cross peak to the 5-CH_3 (Fig. 3 *A*) identifies it as Phe[43](CD1). NOESY peaks from the Phe[43](CD1) $C_\delta Hs$ peak lead to the $C_\alpha HC_\beta H_2$ spin system.[3] The Phe[43](CD1) $C_\epsilon Hs$ also exhibit NOESY cross peaks to the previously assigned $C_{\gamma 1}H_3$ of Val[64](E7) (Fig. 3). Two aromatic side chains located in the COSY spectrum with NOESY cross peaks to Phe[43](CD1) (Fig. 3) identify the pair[3] Phe[33](B14), Phe[46](CD4). They are readily differentiated by the expected NOESY cross peak from Phe[46](CD4) to Val[64](E7) $C_\beta H$. This completes the assignment of the distal residues.

Magnetic axes determination

The location of the magnetic axes makes the explicit assumption that the protein coordinates from the conserved proximal side of the heme are the same as in WT, and that the solution coordinates are the same as those in the single crystal (Rajarathnam et al., 1992, 1993). The conserved proximal structure, moreover, demands conserved WT δ_{dia}. Comparison of x-ray crystal structures among different ligation variants of the same Mb (Bolognesi et al., 1989, 1990; Mattevi et al., 1991), distal point mutants (Carver et al., 1992; Oldfield et al., 1992), as well as a preliminary structure of the analyzed VR-metMb (Rizzi et al., 1993) strongly support this assumption. The orientation of the susceptibility tensor based on three parameter searches fits to Eq. 1 to obtain the Euler angles α, β, γ, relied on the experimentally determined anisotropies of WT metMbCN, $\Delta\chi_{ax} = 1.12 \times 10^{-33}$ m^{-33} and $\Delta\chi_{rh} = 0.376 \times 10^{-33}$ m^{-3}, which have been shown to be valid for several point mutants and genetic variants (Rajarathnam et al., 1992, 1993; Qin et al., 1993). Three different sets of input data were used for VR-metMbCN and VRN-metMbCN.[2] Sets **I** (nine input data) and **II** (14 input data) are based on the proximal side chains shown to accurately reproduce the orientation of the axes for WT metMbCN obtained from much more extensive data sets (Rajarathnam et al., 1992). A larger proximal input data set (18 input shifts; designated here as set **III**) is made possible here because of the additional assignment of the $C_\alpha Hs$ of Gln[91](F6), Ser[92](F7), Ala[94](F9), and $C_\beta H_3$ of Ala[94](F9). The three different input sets **I–III** yield excellent fits to Eq. 1 with low error functions, F/n (Eq. 1), for the three-parameter searches, as shown in Table 3; the previously reported Euler angles and F/n for the same input data sets for WT and V-metMbCN are included for comparison. As was found previously, the resulting Euler angles are remarkably insensitive to the input data sets for both the double and triple mutants, with β invariant, and α and κ ranging over only 2° and 4°, respectively. Moreover, extension of the least square search to five-parameter based on input data set **III** to simultaneously determine α, β, γ and the two anisotropies (data set labeled

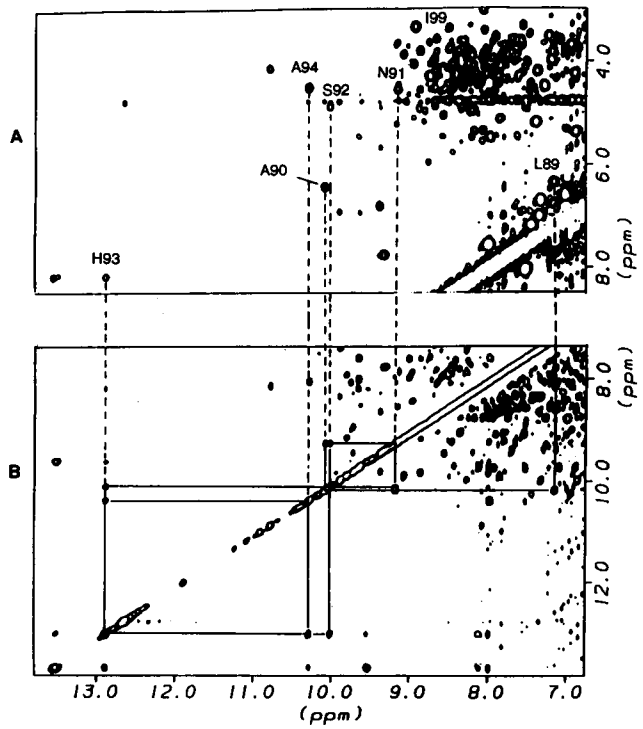

FIGURE 4 A part of the fingerprint region of VR-metMbCN. (*A*) Magnitude COSY in ^1H_2O at 25°C; the identified $C_\alpha H$-NH cross peaks for residues 89–94 (F4–F9 helical segment) are labeled. All the $C_\alpha H$-NH peaks for residue 89–94 (F4–F9 segment) are connected (by *dashed lines*) to (*B*) the NOESY spectrum (mixing time 100 ms) for which the N_iH-$N_{i+1}H$ connectivities from residues 89–94 (F4–F9) are marked by solid lines. The data were processed by applying a 30°-shifted sine-bell-squared window function over 512 t1 and 512 t2 points prior to zero-filling to 2048 × 2048 data points and Fourier transformation.

III′ in Table 3) for the double mutant resulted in negligible changes in the angles and only very small changes in anisotropies (Table 3).

Position of the E helix

The magnetic axes obtained from the 14- or 9-point proximal input data (sets **I** and **II**) for WT metMbCN predicted the distal E helix backbone shifts very well (Rajarathnam et al., 1991). However, as observed in the plot of δ_{dip}(calc) versus δ_{dip}(obs) for VR-metMbCN in Fig. 6, the E helix backbone protons with significant (≥1.5 ppm) δ_{dip}(obs) are poorly predicted (*open circles* in Fig. 6) for the WT coordinates with the error function over the E helix C_αHs (i.e., Eq. 5), F^*/n (E helix C_αHs) = 1.12. Moreover, the ratio of steady-state NOEs[4] from the heme 1-CH_3 and 8-CH_3 to the $C_\alpha H$ of Val^{68}(E11),

$$Q(C_\alpha H) = \frac{\eta(\text{1-CH}_3\text{-E11 C}_\alpha\text{H})}{\eta(\text{8-CH}_3\text{-E11 C}_\alpha\text{H})}, \qquad (6)$$

which is ~1 in WT, is increased to 3.5 for VR-metMbCN. This indicates that the E helix has moved laterally over the heme in the direction of the iron.[5] A similar discrepancy between δ_{dip}(obs) and δ_{dip}(calc) for the E helix backbone, as well as increase in Q(E11 C_αH), were observed for the single point mutant V-metMbCN. A detailed analysis of the influence of a movement of the E helix on both the dipolar shift and Q(E11 C_αH) in the single mutant showed that the E helix moved laterally over the heme by ~0.8 Å in a direction ψ ~80° in Fig. 1 *B* (Rajarathnam et al., 1993). Moving the E helix 0.8 Å in a direction ψ ~80° for VR-metMbCN leads to a significant decrease in the E helix error function, F^*/n(E helix C_αHs) to 0.37; the individual points are shown by the closed circles in Fig. 6.

The highly conserved Phe^{43}(CD1) ring protons are also poorly predicted in VR-metMbCN by WT coordinates (*open squares* in Fig. 6), as was the case in V-metMbCN, with the local error function for the residue (Eq. 5), $F^*(Phe^{43}(CD1))/n$ = 3.34. A similar discrepancy was observed in V-metMbCN and was removed by moving the Phe^{43}(CD1) ring 0.5 Å laterally toward the iron in a direction ψ ~−90° defined in Fig. 1 *B* (Rajarathnam et al., 1993). The same movement of the Phe^{43}(CD1) ring in the present double mutant leads to a much better correlation in Fig. 6 (*closed squares*) and to a vastly superior error function, $F^*(Phe^{43}(CD1))/n$ = 0.54, for the residue (Eq. 5). Hence, we conclude that the E helix and CD corner have readjusted to the double His^{64}(E7) → Val, Thr^{67}(E10) → Arg mutation in essentially the same manner as previously described for the single His^{64}(E7) → Val mutation (Rajarathnam et al., 1993).

Distal side chain orientation

The side chain protons for the substituted residues Val^{64}(E7) and Arg^{67}(E10) in VR-metMbCN exhibit slopes in the plot of chemical shifts versus reciprocal temperature that correlate well with the δ_{dip}(obs) (as shown in Table 2). This indicates that both residues possess well defined orientations in the distal pocket (Emerson and La Mar, 1990b). The conserved Val^{68}(E11), on the other hand, display slopes that are not proportional to δ_{dip}(obs), suggesting an equilibrium among different orientations. The orientation of the substituted Val^{64}(E7) was determined by minimizing the error function (Eq. 5) for the residue, $F^*(Val^{64}(E7))/n$, over the α-β rotational angle. A unique minimum is observed for a HC_α-$C_\beta H$ angle of 180° (not shown) with a good fit, (as shown in Fig. 6 by closed diamonds), and a low error function $F^*(Val^{64}(E7))/n$ = 0.26 for the residue. The orientation of Val^{64}(E7) in VR-metMbCN is the same as that deduced previously for V-metMbCN (Rajarathnam et al., 1993).

The determination of the orientation of Arg^{67}(E10) in VR-metMbCN was pursued along two lines. On the one

[4] Since steady state NOE, $\eta_{(i\to j)} = \sigma_{ij}T_{1j}$, comparison of two NOEs to the same proton j eliminates the dependence of T_{1j}, i.e., $\eta_{(i\to j)}/\eta_{(k\to j)} = \sigma_{ij}/\sigma_{kj} = r_{kj}^6/r_{ij}^6$.

[5] The ratio of NOEs from the heme methyls to Ala^{71}(E14) $C_\beta H_3$ is more difficult to quantitate because of the apparent overlap of the Ala71(E14) $C_\beta H_3$ with another signal that gives an NOE for 1-CH_3.

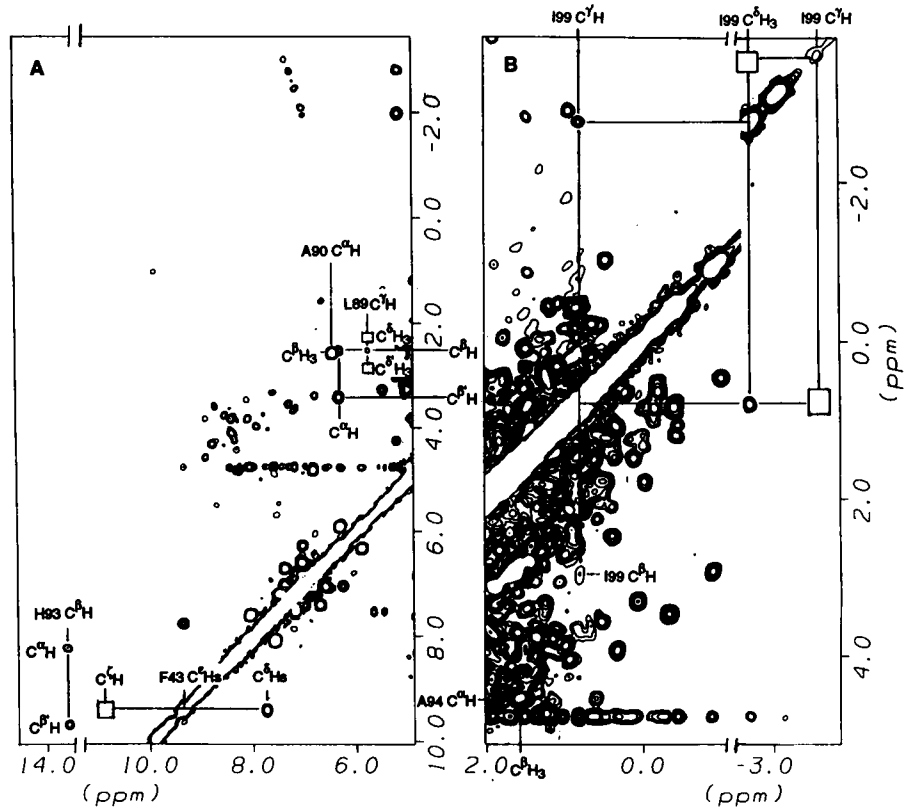

FIGURE 5 Portions of the (*A*) lowfield and (*B*) upfield 500-MHz ^{1}H NMR MCOSY spectrum of VR-metMbCN in ^2H_2O, 0.2 M in NaCl at 25°C, and pH 7.0, illustrating the spin systems for Phe^{43}(CD1), Leu^{89}(F4), Ala^{90}-(F5), and His^{93}(F8) in the lowfield, and Ile^{99}-(FG3) in the highfield window. The data are processed by applying an unshifted sine-bell-squared window over 512 t1 × 512 t2 points prior to zero-filling to 2048 × 2048 data points and Fourier transformation. The boxes indicate cross peaks involving broad signals which are observed by restricting the same window function to only the first 256 t1 × 256 t2 points before zero-filling to 2048 × 2048 and Fourier transformation.

hand, the local error function, $F^*(\text{Arg}^{E10}\text{-CHs})/n$ in Eq. 5, was minimized for the individual C_jHs (j = β, γ, δ) uniquely influenced by rotation about the C_i-C_j bond, starting with the α-β bond. The sequential search for the next bond j-k was carried out starting with the optimized i-j bond angle. The pattern of the $F^*(\text{Arg}^{E10}$ $C_j\text{Hs})/n$ as a function of $\phi_{i\text{-}j}$, is shown in Fig. 7. The last degree of freedom, namely the rotation of the guanidinium group about the C_δ-N_ϵ, bond was limited solely by the requirement that N_ϵH be 4.2 ± 0.2 Å from the iron, as determined from its T_1 value (Travaglini Allocatelli et al., 1993). The resulting plot of δ_{dip}(obs) versus δ_{dip}(calc), shown by open triangles in Fig. 6, leads to a very reasonable correlation for all but N_ϵH, and a reasonable residual $F^*(\text{Arg}^{67}(\text{E10}))/n$ = 0.33 (Eq. 5) for nonlabile protons, and a larger residual $F^*(\text{Arg}^{67}(\text{E10}))/n$ = 2.85 including N_ϵH. The much larger F^*/n for the residue when including N_ϵH is due to the fact that the distance to the iron rather than its dipolar shift was used as a constraint (see Discussion). An alternate assessment of the orientation was made by recognizing that the Arg^{66}(E10) of *A. limacina* Mb is inserted into the heme pocket. Moreover, overlays of the distal pocket coordinates of *A. limacina* and sperm whale Mb indicate good superposition for the heme and E helix backbone (Bolognesi et al., 1990). Hence, the orientation of Arg^{E10} from the *A. limacina* metMbCN complex (Qin et al., 1993) was transferred to VR-metMbCN. The correlation between δ_{dip}-(obs) and δ_{dip}(calc) for this orientation of Arg^{67}(E10) in VR-metMbCN, shown by closed triangles in Fig. 6, is also very reasonable. The residual $F^*(\text{Arg}^{67}(\text{E10}))/n$ = 0.58 (Eq. 5) for the residue excluding N_ϵH, and 2.62 including N_ϵH. Further limited searches failed to significantly improve F^*/n for Arg^{67}(E10) (see Discussion). Both of the orientations of Arg^{67}(E10) determined above have the N_ϵH 4.2 ± 0.2 Å from the iron and in van der Waals contact with the coordinated cyanide ligand, as shown in Fig. 8.

DISCUSSION

Proximal side and heme structure

The assignments for VR-metMbCN presented here are based on standard sequence specific 2D NMR methodology applied routinely in diamagnetic systems (Wüthrich, 1986). The complete spin system for each amino acid in the heme pocket could be traced by bond correlation in spite of linewidth to 80 Hz and T_1 values to 20 ms, and connected to the backbone. The standard N_iH-$N_{i+1}H$, $C_{\beta i}H$-$N_{i+1}H$, $C_{\alpha i}H$-$C_{\beta i+3}H$, and $C_\alpha H$-$N_{i+3}H$ dipolar connectivities place the residue in the sequence (Wüthrich, 1986). While several of the spin systems failed to exhibit remote cross peaks at longer mixing times in TOCSY spectra, the strong temperature dependence of the positions of cross peaks allowed unambiguous tracing of the complete spin systems (Qin and La Mar, 1992). The intra-residue and residue to heme dipolar contacts observed in both VR-metMbCN (Figs. 4 and 5) and VRN-metMbCN (not shown) are essentially the same as observed in WT metMbCN. Moreover, the strongly relaxed protons (i.e., Ile^{99}(FG5) C_γH, His^{97}(FG3) C_4H) exhibit unchanged T_1 values dictating that their position relative to the

TABLE 2 ^{2}H NMR spectral parameters for amino acid residues in sperm whale VR-metMbCN and VRN-metMbCN

Position	Residue	VR-metMbCN						VRN-metMbCN,
		Peak	δ_{obs}*	Slope‡	δ_{dia}§	δ_{dip}(obs)¶	δ_{dip}(calc)‖	δ_{obs}*
43(CD1)	Phe	$C_\delta H_s$	7.70	0.60	7.09	0.61	0.79	8.00
		$C_\epsilon H_s$	9.37	1.21	5.77	3.60	4.78	9.78
		$C_\zeta H$	10.82 (20)	3.62	4.40	6.42	6.12	9.09
63(E6)	Lys**	N_pH	8.58	0.78	8.10	0.48	0.81	8.52
		$C_\alpha H$	4.95	0.95	3.85	1.10	0.56	5.01
64(E7)	Val**	N_pH	9.40	1.12	7.75	1.65	1.49**	9.32
		$C_\alpha H$	6.78	2.16	3.18	3.60	2.91	6.92
		$C_\beta H$	4.81	1.72	1.17	3.64	3.84	4.76
		$C_{\gamma 1}H_3$	8.25 (≤100)	4.22	−0.56	8.81	9.36	8.13
		$C_{\gamma 2}H_3$	3.91	1.55	0.51	3.40	2.90	4.03
65(E8)	Gly**	N_pH	9.74	1.29	8.06	1.68	2.02	9.74
		$C_\alpha H$	4.90	1.42	2.61	2.29	2.44	4.84
		$C_\alpha H'$	4.23		3.25	0.98	1.50	4.62
66(E9)	Val**	N_pH	8.87	0.78	7.32	1.55	0.86	8.77
		$C_\alpha H$	3.81	0.26	3.39	0.42	0.24	3.80
67(E10)	Arg**	N_pH	9.08	1.03	7.86	1.22	0.59	9.09
		$C_\alpha H$	3.88	0.17	4.09	−0.21	−0.42	3.91
		$C_\beta H$	0.89	−0.80	1.98	−1.09	−1.26‡‡	0.86
		$C_\beta H'$	2.02	0.09	1.52	0.50	0.28‡‡	2.26
		$C_\gamma H$	3.93	1.12	0.50	3.43	3.41‡‡	4.25
		$C_\gamma H'$	0.79	0.48	0.50	0.29	0.40‡‡	0.93
		$C_\delta H$	1.71	−0.65	2.40	−0.69	0.38‡‡	2.10
		$C_\delta H'$	3.57	0.50	2.30	1.27	2.41‡‡	3.91
		$N_\epsilon H$	11.25	3.71	1.95	9.30	14.10‡‡	12.51
68(E11)	Val**	N_pH	9.82	1.29	7.81	2.01	1.50	9.86
		$C_\alpha H$	0.99	−1.38	3.49	−2.50	−3.70	0.85
		$C_\beta H$	3.90	1.00	0.58	3.32	3.11	3.58
		$C_{\gamma 1}H_3$	0.29	0.95	0.02	0.27	−0.11	0.00
		$C_{\gamma 2}H_3$	3.39	2.76	−3.05	6.44	5.79	2.80
71(E14)	Ala**	N_pH	6.73	−0.67	7.79	−1.06	−1.78	6.67
		$C_\alpha H$	3.47	−0.78	4.70	−1.23	−1.37	3.46
		$C_\beta H_3$	−0.37	−0.86	2.42	−2.79	−3.10	−0.32
72(E15)	Leu**	N_pH	7.58	−0.39	8.68	−1.10	−1.62	7.58
		$C_\alpha H$	3.36	−0.52	9.13	−0.77	−0.92	3.31
89(F4)	Leu	N_pH	7.16	0.78	6.35	0.81	1.01	7.14
		$C_\alpha H$	6.30	1.64	3.77	2.53	2.69	6.09

* Chemical shifts, in ppm from DSS, in ^2H_2O 0.2 M in NaCl at pH 7.0 and 25°C; T_1s, in ms (uncertainty ± 10%) for strongly relaxed resolved signals are given in parentheses.

‡ Slope of the chemical shifts in a plot of shifts versus reciprocal absolute temperature, in ppm·$\kappa \times 10^4$.

§ Chemical shifts in WT MbCO (Dalvit and Wright, 1987; Chiu, 1992) or as calculated by Eq. 4.

¶ Observed dipolar shift obtained vis Eq. 3.

iron are also strongly conserved. These data, together with the excellent fits of δ_{dip}(obs) and δ_{dip}(calc) for the proximal resonance input data (Table 2), confirm a highly conserved molecular structure of the proximal side of the heme for both the double and triple mutant. The proximal side structure conservation has been confirmed by x-ray crystallography in several Mb point mutants (Carver et al., 1992; Oldfield et al., 1992; Rizzi et al., 1993).

The heme resonance positions in VR-metMbCN and VRN-metMbCN are essentially the same as those of WT and V-metMbCN, indicating a minimally perturbed heme electronic structure. The orbital ground state, and hence rhombic magnetic axes, are not strongly perturbed, as has been found for a variety of other point mutants (Rajarathnam et al., 1992, 1993). The rhombic magnetic axes, defined by κ, range from 25° to 45° among WT and the single, double, and triple point mutants. However, since κ is only weakly reflected in the residual F/n (±10° changes increase F/n only by a factor of 2, while such an increase is produced by only 1° change in β), the variation in κ among the mutants is likely not significant. The VR- and VRN-metMbCN shifts are remarkably similar except for the 6-propionate H_α,H_α' shifts. For VR-metMbCN, as for WT and other mutants, the two 6-propionate H_α peaks exhibit significantly different shifts which reflect the orientation of the side chain necessary to form the salt bridge to Arg^{45}(CD3) (Kuriyan et al., 1986). The change in shift pattern to very similar 6-propionate H_α,H'_α shifts in the triple mutant must reflect the abolition of this salt bridge upon replacing Arg^{45}(CD3) by Asn.

The orientations of the magnetic axes in VR-metMbCN and VRN-metMbCN are as well determined (small total F/n (Eq. 1); highly clustered angles with different input data) as previously reported for WT and several single E7 point mutants (Rajarathnam et al., 1992, 1993). Moreover, extension of the least squares search to include all five parameters did not change the magnetic axes and yielded magnetic anisotropies that are inconsequentially perturbed

TABLE 2 ***Continued***

Position	Residue	VR-metMbCN Peak	δ_{obs}*	Slope‡	δ_{dia}§	δ_{dip}(obs)¶	δ_{dip}(calc)‖	VRN-metMbCN, δ_{obs}* H
90(F5)	Ala	N_pH	10.08	1.47	8.34	1.74	1.94	10.02
		$C_\alpha H$	6.43	1.29	3.44	2.99	3.41	6.40
		$C_\beta H_3$	2.53	0.95	1.17	1.36	1.64	2.54
91(F6)	Gln	N_pH	9.19	0.78	7.87	1.32	1.69	9.08
		$C_\alpha H$	4.56	0.69	3.56	1.00	1.20	4.62
		$C_\beta H$	2.74	0.95	1.90	0.84	0.83	2.70
		$C_\beta H'$	2.83	0.60	2.00	0.83	0.76	2.78
92(F7)	Ser	N_pH	10.02	1.55	7.96	2.06	2.17	9.83
		$C_\alpha H$	4.96	0.80	3.55	1.33	1.22	4.66
		$C_\beta H$	3.77	0.34	3.11	0.66	0.89	4.01
		$C_\beta H'$	4.54	0.41	3.35	1.19	1.13	4.08
93(F8)	His	N_pH	12.91	3.19		-§§	5.11	12.41
		$C_\alpha H$	8.13	2.59		-§§	5.56	7.70
		$C_\beta H$	13.66 (72)	5.52		-§§	8.50	13.12
		$C_\beta H'$	9.66 (125)	2.59		-§§	7.81	9.60
		$C_\delta H$	15.41 (~3)	10.8		-§§	19.5	14.41
		C_2H	−2.43 (~3)	−1.47		-§§	12.7	−2.19
		N_1H	16.96 (28)	3.02		-§§	12.5	16.63
94(F9)	Ala	N_pH	10.29	1.72	7.79	2.50	2.73	10.02
		$C_\alpha H$	4.51	0.43	3.11	1.40	1.28	4.50
		$C_\beta H_3$	1.43	1.03	0.31	1.12	1.17	1.43
97(FG3)	His	$C_\delta H$	8.58 (~20)	3.62	2.34	6.24	6.31	7.66
		C_2H	6.66	−0.78	7.91	−1.25	−1.67	6.55
99(FG5)	Ile	N_p	8.96	0.26	7.92	1.04	0.63	8.88
		$C_\alpha H$	3.36	−0.52	4.29	−0.93	−1.18	3.42
		$C_\beta H$	2.86	1.21	1.37	1.49	1.25	2.98
		$C_\gamma H$	−3.64 (70)	−2.86	−0.28	−3.36	−3.75	−3.57
		$C_\gamma H'$	0.78	0.33	0.35	0.43	0.22	0.60
		$C_\gamma H_3$	−0.98	−1.34	1.36	−2.34	−2.17	−0.76
		$C_\delta H_3$	−2.69	−2.84	1.47	−4.16	−4.11	−2.62
138(H15)	Phe	$C_\delta Hs$	7.12		7.08	0.04	0.05	7.19
		$C_\epsilon Hs$	7.42		7.15	0.27	0.30	7.52
		$C_\zeta Hs$	7.52		7.00	0.52	0.47	7.55

‖ Calculated chemical shifts using Eqs. 1 and 2, $R(-56°, 13.5°, 83°)$ obtained from data set III, and the WT anisotropies, $\Delta\chi_{ax} = 1.12 \times 10^{-33}$ m^{-3}, $\Delta\chi_{rh} = 0.376 \times 10^{-33}$ m^{-3}.

** Assignments for the E helix residue signal and taken from Qin et al., 1993. The δ_{dip}(calc) and δ_{dia} were obtained for the movement of the E helix and optimal orientation of the side chain for Val^{64}(E7), Arg^{67}(E10) and Val^{68}(E11), as described in the text.

‡‡ The δ_{dip}(calc), δ_{dia} for Arg^{67}(E10) is determined by sequential minimizing F^*/n.

§§ The His^{93}(F8) shift contains a large contact contribution, negating the use of Eq. 3. The changes in δ_{obs} from that in WT metMbCN, however, are correctly predicted by the change in δ_{dip}(calc) for the altered magnetic axes.

from those of WT. These results further confirm that the strongly perturbed hyperfine shift patterns in a variety of sperm whale metMbCN mutants can be interpreted by variable orientation of a conserved magnetic susceptibility tensor. This conserved magnetic susceptibility tensor, moreover, is directly supported by the observation of very similar g values in the low temperature EPR spectra of a variety of metMbCN point mutants (Chiu, 1992).

Distal pocket structure

Both the simulation of the dipolar shifts and the large increase in the NOE from the conserved Val^{68}(E11) $C_\alpha H$ to 1-CH_3 relative to that to 8-CH_3 (Eq. 6 for VR-metMbCN), dictate a lateral movement of the E helix in VR-metMbCN toward the iron, in a direction ($\psi \sim 80°$) and with a magnitude (~0.8 Å) as previously described for the single V-metMbCN mutant. Moreover, the Phe^{43}(CD1) moves ~0.5 Å also toward the iron, as found in V-metMbCN (Rajarathnam et al., 1993). The rationale for these movements are likely the same as those proposed for V-metMbCN, namely that the E helix and Phe^{43}(CD1) corner move to fill the void in the pocket that results from the significant reduction of the bulk of the E7 side chain. The fact that the magnitude and direction of the two movements are so similar in the two proteins suggests that the introduction of the Arg^{67}(E10) guanidinium group into the distal pocket occurs without significantly influencing the positions of the conserved residues. Even the substituted Val^{64}(E7) side chain is found here with the same orientation in VR-metMbCN as previously reported for V-metMbCN (Rajarathnam et al., 1993). A similar situation has been discussed for *A. limacina* Mb, where essentially the same heme pocket structure is observed in a crystal whether Arg^{E10} is oriented into the pocket or out to the protein surface (Bolognesi et al., 1989, 1990; Mattevi et al., 1991; Conti et al., 1993). The very similar δ_{obs} for VR-metMbCN and VRN-metMbCN (Table 2), in particular for the Val^{64}(E7), Arg^{67}(E10), and Phe^{43}(CD1) residues, and the essentially indistinguishable magnetic axes (Table 3), indicate that VRN-metMbCN exhibits the same structural accom-

TABLE 3 Orientation of magnetic axes and error functions for sperm whale mutant and WT metMbCN

Input data sets*			Euler angle			Error function¶
Code‡	n‡	$\overline{\delta_{dip}}$ §	α	β	$\kappa(=\alpha+\gamma)$	F/n (Eq. 1)
Wild type‖						
I	14	3.23	9	16.0	39	0.055
II	9	4.49	10	16.0	36	0.057
V-metMbCN**						
I	14	2.39	-27	14.5	45	0.054
II	9	3.08	-28	14.5	45	0.054
VR-metMbCN						
I	14	2.03	-56	13.5	25	0.054
II	9	2.60	-56	13.5	29	0.043
III	18	2.04	-56	13.5	27	0.052
III′	18	2.04	-56	13.5	29	0.036
VRN-metMbCN						
I	14	2.00	-60	15.0	25	0.063
II	9	2.56	-58	15.0	29	0.046
III	18	1.95	-59	15.0	25	0.058

* All data are for three-parameter least-squares fits to obtain an α, β, γ, using the WT metMbCN anisotropies, $\Delta\chi_{ax} = 1.12 \times 10^{-33}$ m^{-3} and $\Delta\chi_{rh} = 0.376 \times 10^{-33}$ m^{-3}, except for that labeled **III′**, which consists of a five-parameter search to obtain both Euler angles and magnetic anisotropies; the optimum anisotropies, for **III′**, $\Delta\chi_{ax} = 1.08 \times 10^{-33}$ m^{-3}, $\Delta\chi_{rh} = 0.396 \times 10^{-33}$ m^{-3}, are very close to those of WT.

‡ Input data sets defined in footnote 3.

§ The mean observed dipolar shift $\overline{\delta_{dip}} = (1/n) \sum | \delta_{dip}(obs) |$.

¶ Residual error function, in ppm^2, as given by Eq. 1.

‖ Taken from Rajarathnam et al. (1992).

** Taken from Rajarathnam et al. (1993).

modation in the distal pocket relative to WT as does VR-metMbCN. The additional substitution of Arg^{45}(CD3) →Asn, which must abolish the 6-propionate-Arg CD3 link, does not appear to affect the distal pocket structure. This may not be surprising, since the crystal structure of WT MbCO finds partial occupation of a form with the Arg^{45}(CD3)-6-propionate salt bridge broken (Kuriyan et al., 1986).

The two approaches used to estimate the orientation of Arg^{67}(E10) in VR-metMbCN yield δ_{dip}(calc) which result in similar residual error functions (Eq. 5) for the residue, F^*/n (0.37, 0.55 for nonlabile protons, and 2.89, 2.62 including $N_\epsilon H$), with both exhibiting significant deviation only for the resolved labile $N_\epsilon H$ proton. What is remarkable about the orientations deduced by the two alternate approaches, sequential optimization of each bond angle, and transfer of the Arg^{E10} side chain from *A. limacina* Mb (Qin et al., 1993), is the similarity of the results. The mean difference in position, in angstroms, for the side chain carbons (excluding the guanidinium group) in the two orientations is only 0.30 Å (range, 0.21–0.40 Å and 0.26 Å for C_δ), and for the nonlabile side chain protons is only 0.32 (range, 0.16–0.47 and ~0.3 Å for $C_\delta Hs$). Hence the two alternate approaches yield essentially the same orientation for the $C_\alpha H$-$C_\beta H_2$-$C_\delta H_2$-$C_\delta H_2$ portion of Arg^{67}(E10). With only such small differences in the orientation between the two approaches, it was not deemed worthwhile to further optimize the orientation.

For the guanidinium group, N_ϵ and H_ϵ differ in position for the two orientations by 0.24 and 0.15 Å, respectively, and hence the position of this proton (H_ϵ), which also forms a hydrogen bond to the bound ligand, is as well-defined as the remainder of the carbon chain. The distance between Arg^{67}(E10) $N_\epsilon H$ and Val^{64}(E7) $C_\gamma H_3$, r ~3.2 Å, obtained for this orientation deduced from the dipolar shift, is consistent[6] with the ~–6% NOE previously reported for Val^{64}(E7) $C_{\gamma 1}H_3$ upon saturation Arg^{67}(E10) $N_\epsilon H$ (Travaglini Allocatelli et al., 1993). The difference in position between the two Arg^{67}(E10) orientations are larger for the $N_\xi H_2$ group oriented toward the iron-bound ligand (0.61 Å for $N_{\xi 1}$ and 0.52, 0.85 Å for Hs) than for the group oriented away from the iron (0.85 Å for $N_{\xi 2}$ and 1.1, 0.9 Å for Hs). The difference between the Arg^{67}(E10) orientations deduced by the two approaches are somewhat larger for the guanidinium group, which is not surprising, since NMR constraints are available only for the $N_\epsilon H$ (δ_{dip}(obs), R_{Fe} from T_1) which is close to the well-defined C_δ position.

The alternate orientations for Arg^{67}(E10) predict large dipolar shifts for one $N_{1\xi}H$ (to appear in the 15–25-ppm window), the one that likely also hydrogen bonds to the ligand. No such additional hyperfine shifted and relaxed proton signals could be found in the ^{1}H NMR spectrum. This discrepancy can have two likely origins. On the one hand, the $N_\xi H_2$ group may be reorientating so as to yield either undetectable exchange-broadened lines or an averaged signal that is not resolved from the intense diamagnetic envelope. Broadened $N_\xi Hs$ signals due to reorientation of the NH_2 group of a hyperfine-shifted Arg guanidinium group have been observed in *Chironomus* monomeric metHbCN (Peyton et al., 1991). On the other hand, the predicted chemical shifts for the labile protons near the iron have much larger uncertainties than for more remote nonlabile protons. This is due to

[6] Steady state NOE, $\eta_{i\text{-}j} = \sigma_{ij}T_{1j}$, where $\sigma_{ij} = -0.1\gamma^2\hbar^4 r_{ij}^{-6}\tau_c$ and τ_c for a 17-kDa protein is estimated as 9 ns.

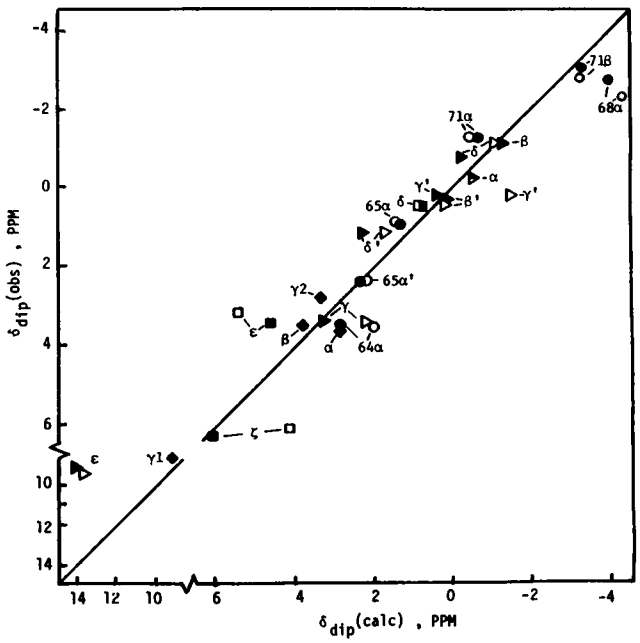

FIGURE 6 Plot of δ_{dip}(obs) (obtained via Eq. 3) versus δ_{dip}(calc) (obtained via Eq. 2) for dipolar-shifted distal residue signals. The E helix backbone protons with significant (>1 ppm) dipolar shift for C_αHs of Val^{64}(E7), Gly^{65}(E8), Val^{68}(E11), Ala^{71}(E14), and $C_\beta H_3$ of Ala^{71}(E14) for the WT coordinates of the E helix (*open circles*) are labeled by position, and upon moving the E helix laterally 0.8 Å in the direction given by $\psi \sim 80°$ in Fig. 1 (*closed circles*). The Phe^{43}(CD1) ring proton for the WT coordinates (*open squares*) labeled by positions, and upon moving the ring 0.5 Å in the direction $\psi = -90°$ shown in Fig. 1 *B* (*closed squares*). The data points for Val^{64}(E7) upon minimizing the error function $F^*(Val^{64}(E7))/n$ over α-β bond rotation, are shown in closed diamonds and labeled by position. The open triangles and closed triangles (labeled by position) represent the data for the orientation of Arg^{66}(E10) obtained by sequentially minimizing $F^*(C_jHs))/n$ over *i-j* bond rotation, and that taken from the orientation of Arg^{66}(E10) in the *A. limacina* metMbCN structure (Qin et al., 1993), respectively.

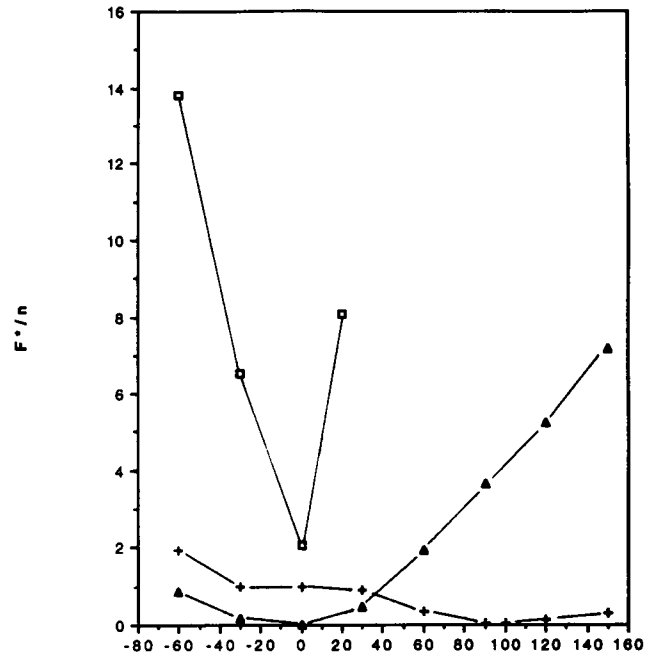

FIGURE 7 Plot of $F^*(C_jHs))/n$ (j = β, γ, δ) as a function of *i-j* bond rotation for Arg^{67}(E10) in the magnetic coordinate system $R(-56°, 13.5°, 83°)$, with $\Delta\chi_{ax} = 1.12 \times 10^{-33}$ m^{-3}, $\Delta\chi_{rh} = 0.376 \times 10^{-33}$ m^{-3}. The α-β bond is rotated first to optimize C_βHs, and the C_β-C_γ rotation is carried out at the optimized α-β bond, etc. The symbols +, △, and □ represent the sequential rotations about the α-β, β-γ, and γ-δ bonds, respectively.

the fact that both the diamagnetic ring current effects (Eq. 4) and dipolar shifts (Eq. 2) are each extraordinarily sensitive to small displacements close to the iron, and these two contributions to the observed shift are in opposite directions. Hence moderate uncertainties in δ_{dip}(calc) and δ_{dia} can lead to very poorly predicted observed shifts for labile protons. Nevertheless, the two orientations agree remarkably well in placing two protons in hydrogen bonding distance of the bound cyanide, with the $N_\epsilon H$ producing a resolved signal.

Orientation of the major magnetic axis/ligand tilt

Detailed analysis of variable input sets and the sensitivity of the residual error function on the various angles has shown that the described procedures yield the orientation of the magnetic axes with β (tilt magnitude) reliable to ±1°, α (the tilt direction) reliable to ±10°, and κ (= $\alpha + \gamma$) (the rhombic axes) reliable to ±10° (Rajarathnam et al., 1993, 1993; Qin et al., 1993). Hence, β does not differ significantly between V-metMbCN (Rajarathnam et al., 1993) and the present mutants of interest, VR-metMbCN, VRN-metMbCN. However, α is more negative by ~25° in the latter two proteins, and this change is outside the uncertainty range. The magnitude and the direction of the *z*-axis tilt (-*z*-axis; see Fig. 1), in WT metMbCN agrees well with the Fe-C tilt in MbCO crystals (Cheng and Schoenborn, 1991), and hence the tilt of the major magnetic axis is directly correlated with, and attributable to, the tilt of the Fe-CN unit from the heme normal. More accurately, the magnetic *z* axis would measure the Fe-C tilt (Rajarathnam et al., 1993; Qin et al., 1993). In two cases, spectroscopic studies of Fe-CN in metMbCN and metHbCN have suggested that the Fe-CN unit, unlike the Fe-CO unit, is essentially linear (Bianconi et al., 1985; Yu et al., 1984).

Previous detailed ^{1}H NMR studies of the V-metMbCN single mutant showed that, while the tilt magnitude (14.5°) is insignificantly altered from that in WT metMbCN (16°), the direction of Fe-CN tilt is strongly rotated by ~40° from a direction toward β-meso-H in WT, to one toward pyrrole III in V-metMbCN (Fig. 1 *B*) (Rajarathnam et al., 1993). Moreover, the conserved tilt magnitude but changed tilt direction, could be rationalized on the basis of available energy contour diagrams for the O atom of the Fe-CO unit in the heme pocket of WT MbCO (Kuriyan et al., 1986) and that with His^{64}(E7) rotated out of the heme pocket (a reasonable model for V-MbCO). The orientation of the magnetic axes for the double VR-metMbCN and triple VRN-metMbCN mutants are indistinguishable. However, both differ from that

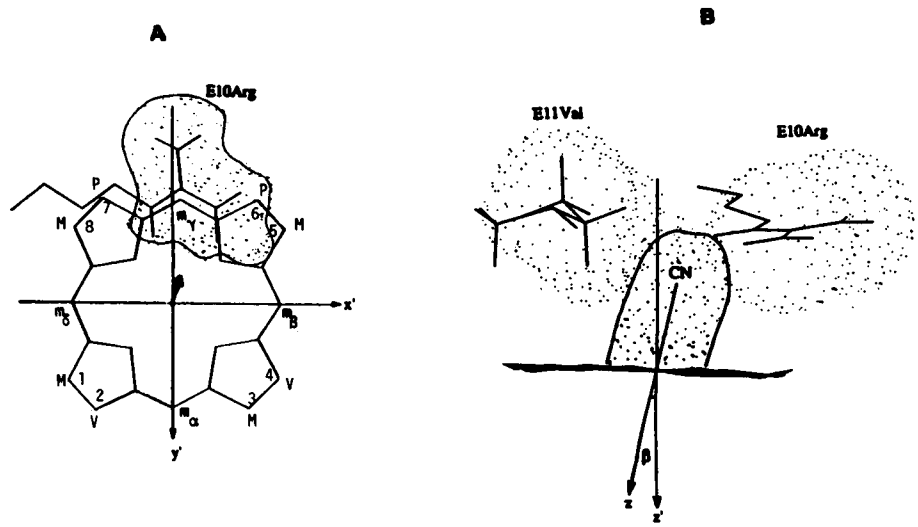

FIGURE 8 The dispositions of heme Arg^{67}(E10) side chain for VR-metMbCN as determined from ^1H NMR data. (*A*) Face-on view from the distal side. The van der Waals surface for the Arg^{67}(E10) guanidinium group is in contact with that of the bound cyanide. (*B*) Edge-on view from the δ-meso-H direction for the dispositions of distal Val^{E11}, Arg^{E10}, and proposed cyanide ligand orientation. The ligand is tilted approximately towards the γ-meso-H direction which appears to favor the H-bonding with Arg^{67}(E10).

of V-metMbCN in exhibiting a further rotation (by an additional 25°) of the direction of tilt (α) toward the γ-meso-H position (Fig. 1 *B*); the tilt magnitude in the three mutants are essentially constant at 14.0 ± 1.0°. Since the dispositions of residues Phe^{43}(CD1) and Val^{64}(E7) are the same in the single, double, or triple mutants, it is unlikely that the further rotation of the tilted Fe-CN unit results from increased steric interaction between the bound ligand and either Phe^{43}(CD1) or Val^{64}(E7) in the double or triple mutant. On the other hand, the direction of rotation of the Fe-CN unit in the double or triple mutant relative to that in the single mutant is to place the terminal nitrogen of the bound cyanide closer to the Arg^{67}(E10) guanidinium group and in hydrogen bonding distance to $N_\epsilon H$. Hence the direction of the ligand tilt (or major magnetic axis) is consistent with an attractive interaction between the Arg^{67}(E10) side chain and the ligand due to hydrogen bonding. Such hydrogen-bonding had been previously documented by the observation of a significant solvent isotope effect on the heme hyperfine shifts (Travaglini Allocatelli, et al., 1993). This geometry of the ligand tilt and the interaction with the Arg^{67}(E10) side chain are illustrated by their van der Waals surfaces depicted in Fig. 8.

CONCLUSIONS

The hyperfine shift pattern for the signals for noncoordinated residues of the structurally conserved proximal side allow the quantitative determination of the magnetic axis, and hence tilt of the ligand, for the VR double and VRN triple point mutants of sperm whale metMbCN. The magnetic axes, together with NOE constraints, show that the E helix and Phe CD1 have moved 0.5–0.8 Å toward the iron in a manner very similar to that described for the single V-metMbCN mutant, and allow the determination of the orientation of the substituted Val^{E7} and Arg^{E10} residue in VR-metMbCN. Arg^{67}(E10) is oriented into the heme pocket and its guanidinium group participates in hydrogen bonding interactions with the coordinated cyanide. The change in the direction of the ligand tilt in the VR and VRN mutants from that in V-metMbCN is attributed to an attractive hydrogen bonding interaction between Arg^{E10} and the bound cyanide.

We are indebted to S. D. Emerson for the computer program used in the determination of magnetic axes, and to A. D. McPherson for modifications of these programs. Useful discussions with K. Rajarathnam and K. Vyas are acknowledged.

This research was supported by grants from the National Institutes of Health, HL 16087 (to G. N. La Mar) and from Italian Agencies Ministero dell'Università e Ricerca Scientifica e Technologica (40% "LIVEPROTEIN") and CNR 91.0222.CT04. The NMR instrumentation was purchased, in part, with funds provided by grants from the National Institutes of Health, RR-04795, and the National Science Foundation, BBS-88-04739.

REFERENCES

Bax, A., and D. G. Davis. 1985. MLEV-based two-dimensional homonuclear magnetization transfer spectroscopy. *J. Magn. Reson.* 65: 355–360.

Bax, A. 1984. Two-Dimensional Nuclear Magnetic Resonance in Liquids. Delft University Press, Delft, Dordrecht, the Netherlands. 50–98.

Bax, A., R. Freeman, and G. Morris. 1981. Correlation of proton chemical shifts by two-dimensional Fourier transform NMR. *J. Magn. Reson.* 42: 164–168.

Bellelli, A., G. Antonini, M. Brunori, B. A. Springer, and S. G. Sligar. 1990. Ligand binding to a hemoprotein lacking the distal histidine. *J. Biol. Chem.* 265:18898–18901.

Bianconi, A., A. Congiu-Castellano, P. J. Durham, S. S. Hasnain, and S. Philips. 1985. The CO bond angle of carboxymyoglobin determined by angular-resolved XANES spectroscopy. *Nature (Lond.).* 318:685–687.

Bolognesi, M., A. Coda, F. Frigerio, G. Gatti, P. Ascenzi, and M. Brunori. 1990. X-ray crystal structure of the fluoride derivative of *Aplysia limacina* ferric myoglobin at 2.0 Å resolution. *J. Mol. Biol.* 225:621–625.

Bolognesi, M., S. Onesti, G. Gatti, A. Coda, P. Ascenzi, A. Giacometti, and M. Brunori. 1989. *Aplysia limacina* myoglobin crystallographic analysis at 1.6 Å resolution. *J. Mol. Biol.* 205:529–544.

Braunschweiler, L., and R. R. Ernst. 1983. Coherence transfer by isotropic mixing: application to proton correlation spectroscopy. *J. Magn. Reson.* 53:521–528.

Carver, T. E., R. E. Brantley, E. W. Singleton, R. M. Arduini, M. L. Quillen, G. N. Phillips, Jr., and J. S. Olson. 1992. A novel site-directed mutant of myoglobin with an unusually high O_2 affinity and low autooxidation rate. *J. Biol. Chem.* 267:14443–14450.

Cheng, X., and B. P. Schoenborn. 1991. Neutron diffraction study of carbonmonoxymyoglobin. *J. Mol. Biol.* 220:381–399.

Chiu, M. L. 1992. Structure and dynamics of myoglobin and its mutants. Ph.D. thesis. University of Illinois, Urbana.

Collman, J. P., J. I. Brauman, T. R. Halbert, and K. Suslick. 1976. Nature of O_2 and CO binding to metalloporphyrins and heme proteins. *Proc. Natl. Acad. Sci. USA.* 73:3333–3337.

Conti, C., C. Moser, M. Rizzi, A. Mattevi, C. Lionetti, A. Coda, P. Ascenzi, M. Brunori, and M. Bolognesi. 1993. X-ray crystal structure of ferric *Aplysia limacina* myoglobin in different ligand states. *J. Mol. Biol.* In press.

Cross, K. J., and P. E. Wright. 1985. Calibration of ring-current models for the heme ring. *J. Magn. Reson.* 64:220–231.

Cutruzzolá, F., C. Travaglini Allocatelli, P. Ascenzi, M. Bolognesi, S. G. Sligar, and M. Brunori. 1991. Control and recognition of anionic ligands in myoglobin. *FEBS Lett.* 282:218–284.

Dalvit, C., and P. E. Wright. 1987. Assignment of resonances in the ^1H nuclear magnetic resonance spectrum of the carbon monoxide complex of sperm whale myoglobin by phase-sensitive two-dimensional techniques. *J. Mol. Biol.* 194:313–327.

Davis, D. G., and A. Bax. 1985. Assignment of complex ^1H NMR spectra via two-dimensional homonuclear Hartmann-Hahn spectroscopy. *J. Am. Chem. Soc.* 107:2820–2821.

Emerson, S. D., and G. N. La Mar. 1990a. Solution structural characterization of cyanomet myoglobin: resonance assignment of heme cavity residues by two dimensional NMR. *Biochemistry.* 29:1545–1556.

Emerson, S. D., and G. N. La Mar. 1990b. NMR determination of the orientation of the magnetic susceptibility tensor of cyano metmyoglobin: a new probe of steric tilt of bound ligand. *Biochemistry.* 29:1556–1566.

Jeener, J., B. H. Meier, P. Bachmann, and R. R. Ernst. 1979. Investigation of exchange processes by two dimensional NMR spectroscopy. *J. Chem. Phys.* 71:4546–4553.

Kuriyan, J., S. Witz, M. Karplus, and G. A. Petsko. 1986. X-ray structure and refinement of carbon-monoxy (Fe^{II})-myoglobin at 1.5 Å resolution. *J. Mol. Biol.* 192:133–154.

Lecomte, J. T. J., and G. N. La Mar. 1987. ^1H NMR probe for hydrogen bonding of distal residues to bound ligands in heme proteins: isotope effect on heme electronic structure of myoglobin. *J. Am. Chem. Soc.* 109:7219–7220.

Mattevi, A., G. Gaffi, A. Coda, M. Rizzi, P. Ascenzi, M. Brunori, and M. Bolognesi. 1991. Binding mode of azide to ferric *Aplysia limacina* myoglobin. Crystallographic analysis at 1.9 Å resolution. *J. Mol. Recognition.* 4:1–6.

Oldfield, T. J., S. J. Smerdon, Z. Dauter, K. Petratos, K. S. Wilson, and A. J. Wilkinson. 1992. High-resolution x-ray structure of pig metmyoglobin and two CD3 mutants, Mb(Lys^{45}→Arg) and Mb(Lys^{45}→Ser). *Biochemistry.* 31:8732–8739.

Peyton, D. H., G. N. La Mar, S. Ramaprasad, S. Unger, S. Sankar, and K. Gersonde. 1991. Proton nuclear magnetic resonance study of the solution distal histidine orientation in monomeric *Chironomus thummi thummi* cyanomet hemoglobins. *J. Mol. Biol.* 221:1015–1026.

Phillips, S. E. V., and B. P. Schoenborn. 1981. Neutron diffraction reveals oxygen-histidine hydrogen bond in oxymyoglobin. *Nature (Lond.).* 292: 81–82.

Phillips, S. E. V. 1980. Structure and refinement of oxymyoglobin at 1.6 Å resolution. *J. Mol. Biol.* 142:531–554.

Qin, J., and G. N. La Mar. 1992. Complete sequence-specfic assignment of hyperfine-shifted residues in the active site of a paramagnetic protein: application to cyano-met *Aplysia* myoglobin. *J. Biomolecular NMR.* 2:597–618.

Qin, J., G. N. La Mar, F. Ascoli, M. Bolognesi, and M. Brunori. 1992. Solution ^1H NMR resonance determination of hydrogen-bonding of the E10 (66) Arg side chain to the bound ligand in *Aplysia* cyano-met myoglobin. *J. Mol. Biol.* 224:891–897.

Qin, J., G. N. La Mar, F. Ascoli, and M. Brunori. 1993. Solution NMR determination of active site structure for a paramagnetic protein: cyanomet *Aplysia* Mb. *J. Mol. Biol.* 231:2009–1023.

Rajarathnam, K., G. N. La Mar, M. Chiu, and S. G. Sligar. 1992. Determination of the orientation of the magnetic axes of the cyano-met complexes of point mutants of myoglobin by solution ^1H NMR: influence of His E7 → Gly and Agr CD3 →Gly substitutions. *J. Am. Chem. Soc.* 114:9048–9058.

Rajarathnam, K., J. Qin, G. N. La Mar, M. Chiu, and S. G. Sligar. 1993. Solution structure determination of the heme cavity in the E7 His → Val cyano-met myoglobin point mutant based on the ^1H NMR detected dipolar field of the iron: evidence for contraction of the heme pocket. *Biochemistry.* 32:5670–5680.

Rance, M. 1987. Improved techniques for homonuclear rotation-frame and isotropic mixing experiments. *J. Magn. Reson.* 74:557–564.

Rizzi, M., M. Bolognesi, A. Coda, F. Cutruzzolá, C. Travaglini Allocatelli, A. Brancaccio, and M. Brunori. 1993. Crystal structure of a distal site double mutant of sperm whale myoglobin at 1.6 Å resolution. *FEBS Lett.* 320:13–16.

Springer, B. A., K. D. Egeberg, S. G. Sligar, R. J. Rohlfs, A. J., Mathews, and J. S. Olson. 1989. Descrimination between oxygen and carbon monoxide and inhibition of autoxidation by myoglobins. *J. Biol. Chem.* 264: 3057–3060.

States, D. J., R. A. Haberkorn, and D. J. Reuben. 1982. A two-dimensional nuclear Overhauser experiment with pure absorption phase in four quadrants. *J. Magn. Reson.* 48:286–292.

Travaglini Allocatelli, C., F. Cutruzzolá, A. Brancaccio, M. Brunori, J. Qin, and G. N. La Mar. 1993. Structural and functional characterization of sperm whale myoglobin mutants: role of arginine (E10) in ligand stabilization. *Biochemistry.* 32:6041–6049.

Wishart, D. S., B. D. Sykes, and F. M. Richards. 1991. Relationship between nuclear magnetic resonance chemical shift and protein secondary structure. *J. Mol. Biol.* 222:311–333.

Wittenberg, B. A., M. Brunori, E. Antonini, J. B. Wittenberg, and J. Wyman. 1965. Functional properties of *Aplysia limacina* myoglobin. *Arch. Biochem. Biophys.* 111:576–579.

Wüthrich, K. 1986. NMR of Proteins and Nucleic Acids. Wiley, New York.

Yu, L. P., G. N. La Mar, and K. Rajarathnam. 1990. ^1H NMR resonance assignment of the active site residues of paramagnetic protein by 2D bond correlation spectroscopy: metcyano myoglobin. *J. Am. Chem. Soc.* 112: 9527–9534.

Yu, N.-T., B. Benko, E. A. Kerr, and K. Gersonde. 1984. Iron-carbon bond lengths in carbonmonoxy and cyanomet complexes of the monomeric hemoglobin III from *Chironomus thummi thummi*: a critical comparison between resonance Raman and x-ray diffraction studies. *Proc. Natl. Acad. Sci. USA.* 81:5106–5110.